Photodissociation of water using colloidal nanoparticles of doped titanium (IV) oxide semiconductors for hydrogen production

Kasem K. Kasem* and Melissa Dahn

Natural Information and Mathematical Sciences Department, School of Art and Sciences, Indiana University Kokomo, Kokomo, IN 46904, USA

Selective photo-production of hydrogen was achieved with visible range solar radiation without application of any external potential. Aqueous solutions of TiO_2 doped with different percentages of V_2O_5 were used to maximize the absorption of visible light. The effects of the hole-scavengers such as poly-anions and solvated-electron suppliers were studied. Studies show that in phosphate buffer, 5% V_2O_5 generated maximum photocurrent. Potassium ferrocyanide gives the most promising results as a solvated-electron supplier and electron exchanger in basic phosphate buffer. The aqueous nanosystems that we used retained their stability as indicated by the reproducibility of their photocatalytic activities. Solar-radiated assemblies of doped $TiO_2/[Fe(CN)_6]^{4-}$ sustained cyclic systems for continuous hydrogen production.

Keywords: Aqueous colloids, hydrogen, nanoparticles, semiconductors, titanium oxide.

PHOTOCHEMICAL cleavage of water into hydrogen and oxygen using semiconductor mediators have been reported[1–11]. Ordered assemblies of narrow band gap semiconductor nanostructures are convenient systems to study visible light energy. Several procedures were adopted to prepare these assemblies. In most of them, one material with a specific band gap is produced. Studies were performed on metal chalcogenides such as sulphides, selenides and tellurides, but low conversion efficiencies were reported[12–20]. The photocurrent obtained using such nano-sized assemblies is often low, as fast charge recombination limits photocurrent generation. When composite semiconductors are used, it is possible to improve the efficiency of charge separation through charge rectification. This can take place by modifying either the surface of the base semiconductor, or its composition, with either inorganic or organic semiconductors.

Although most of the studies on the photo-dissociation of water took place over compact semiconductor electrodes, in some studies particle-size semiconductors were used because of the larger surface area and their ability to carry out all the reactions that were previously associated with semiconductor electrodes. A platinized semiconductor powder such as TiO_2 is an example of the case for simultaneous production of oxygen and hydrogen. The spatial separation between oxidative and reductive sites is small and increases the back reactions.

TiO_2 (titania) is known as a photocatalysis agent for a wide range of substances[21]. Nano-sized TiO_2 possesses enhanced photocatalytic activity and solar energy conversion[22,23]. However, some disadvantages limit the efficient use of TiO_2, for example, the high band gap energy (3.2 eV) requires UV radiation for photo-activation limiting its application in the visible light range, and charge carrier recombination (e^-/h^+) occurs within nanoseconds limiting its photocatalytic activity[24]. TiO_2 was used to host some rare-earth doping due to its properties such as mechanical stability[25]. On the other hand, the major advantage of TiO_2 is its stability in aqueous solutions. Doping TiO_2 with some transition metal oxides of low band gap may lower the band-gap energy and alter the photonic activities by lowering the (e^-/h^+) recombination process.

Effective conversion of solar energy to hydrogen requires an inexpensive source that contains hydrogen and a large surface area. Aqueous colloidal nanoparticle suspensions meet these requirements.

In addition to the importance of the suspension particles, the suspension medium is equally important in generating an efficient photolysis process. Earlier studies used semiconductor particles as major producers of photonic outcome through heterogeneous charge transfer processes at the particle/electrolyte interface[18,26,27]. Hydrated electrons can play an important role in photo-dissociation of water through the following reactions:

$$[Fe(CN)_6]^{4-} + h\nu = [Fe(CN)_6]^{3-} + e_{aq^-}, \quad (1)$$

$$e_{aq^-} + e_{aq^-} = H_2 + 2OH^-. \quad (2)$$

The second reaction (eq. (2)) proceeds with a rate $k \approx 1 \times 10^{10}\ M^{-1}\ s^{-1}$ (ref. 28). The molecular orbital structure of hexacyano iron (II) $[Fe(CN)_6]^{4-}$ allows electronic transitions under the photo-excitation condition and produces hydrated electrons that react according to the above reactions. $[Fe(CN)_6]^{4-}$ undergoes oxidation to $[Fe(CN)_6]^{3-}$. The oxidation process compromises of the reported high rate of hydrated electrons reactions. The disadvantage of a homogeneous process for hydrogen production is its irreversibility. However, this can be overcome by the use of a semiconductor system which acts as an electron donor and reduces $[Fe(CN)_6]^{3-}$ back to $[Fe(CN)_6]^{4-}$. Achieving such a goal will create the conditions of reversible ergo-dynamics. The perfect conditions could be reached if the rate of reduction of $[Fe(CN)_6]^{3-}$ was closer to the rate of formation of hydrated electrons from $[Fe(CN)_6]^{4-}$.

A means to lower the TiO_2 band gap for efficient capture of visible radiation is doping TiO_2 with some 3d metal oxides.

*For correspondence. (e-mail: kkasem@iuk.edu)

In this communication, we study the effect of V^{+5} on the band gap of TiO_2 containing V_2O_5, and further on the photocatalytic behaviour of TiO_2 suspensions in buffered ferrocyanide solutions (as the hydrated electron supplier). Different concentrations of V_2O_5 as a dopant for TiO_2 colloidal nanoparticles were used to find the effect on the rate of hydrogen production. The possibility of using these systems in solar energy-based photolysis cells that achieve the goal of efficient reversible cyclic processes for hydrogen production was explored. The effect of some poly anions on the selectivity of the photolysis process towards hydrogen production has also been explored.

All the reagents used were of analytical grade. All the solutions were prepared using deionized water, unless otherwise stated. TiO_2 doped with V_2O_5 was prepared following a procedure similar to that described elsewhere[29]. We used $NaVO_3$ as a source of dopant in quantities that generate 5%, 10% and 15% of V_2O_5 in TiO_2 samples.

All electrochemical experiments were carried out using a conventional three-electrode cell consisting of Pt wire as a counter electrode, Ag/AgCl as a reference electrode, and Pt gauze as an electron collector. A BAS 100 W electrochemical analyser (Bioanalytical Co) was used to perform the electrochemical studies. Steady-state reflectance spectra were recorded using Shimadzu UV-2101 PC. An Olympus BX-FLA60 reflected light fluorescence microscope working with polarized light at a wavelength (λ) range between 330 and 550 nm was used to make sure that the size of colloidal particles did not exceed 200 nm.

The electrolysis cell was a 120 ml, single-compartment Pyrex cell with a quartz window facing the irradiation source. A 10 cm^2 platinum gauze cylinder was used as a working electrode. Aqueous suspensions were stirred with a magnetic stirrer during the measurements. The cell design is displayed in Figure 1. An $Ag/AgCl/Cl^-$ reference electrode was also fitted into this compartment. A 10 cm^2 platinum counter electrode was housed in a glass cylinder sealed at one end with a fine-porosity glass frit. The pH was adjusted by addition of either 1 M NaOH or 1 M HNO_3.

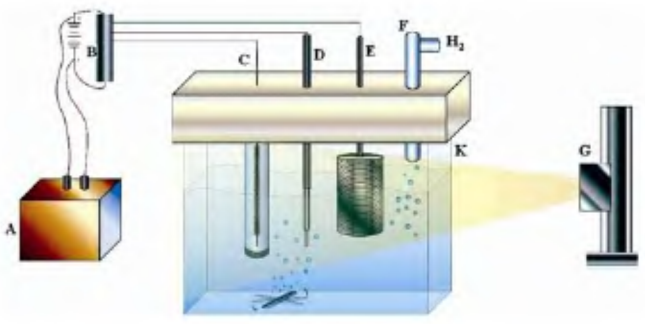

Figure 1. Photolysis cell. A, Photovoltaic generator; B, Light-powered potentiostat; C, Counter electrode; D, Reference electrode; E, Collector electrode; F, Gas outlet; G, Solar simulator and K, Cell glass body.

Irradiations were performed with a solar simulator 300 W xenon lamp (Newport) with an IR filter. Light was focused on the cell window using a metal cylinder with 5 cm diameter and 15 cm length. The cell position was adjusted to allow full illumination of the 100 ml suspension. Photolysis of $[Fe(CN)_6]^{4-}$ will generate hydrated electrons and $[Fe(CN)_6]^{3-}$. The potential of the working electrode was fixed at 100 mV more negative than the reduction potential of $[Fe(CN)_6]^{3-}$ to guarantee full reduction of ferricyanide. The current due to the reduction of $[Fe(CN)_6]^{3-}$ collected by the working electrode during the photolysis process is a measure of the photocurrent. Photocurrent–time curves were obtained with a BAS 100 W bio-analytical system. The measured photocurrent was normalized to $Am^{-2}\ h^{-1}$ (ampere per square metre per hour) of illumination. Both the amorphous and catalytic nature of the 3d metal oxide nanoparticles significantly reduces hydrogen over voltage[30]. Because the measured photocurrent is a function of regeneration of ferrocyanide (the solvated electron suppliers that generate hydrogen), the measured photocurrent was normalized considering two photons per one hydrogen molecule (according to eq. (2)), and was used to calculate the number of moles of hydrogen generated per square metre per hour of illumination. In these calculations, hydrogen production generated at the semiconductor/electrolyte interface and that generated via the mechanical effects of the magnetic stirrer were ignored[31]. Although hydrogen was detected using HY-ALERTA^{TM} 500 (h2 scan California), a flame test was used to confirm that the gas bubbles generated by irradiation were composed of hydrogen and not HCN. There was no evidence of the discolouration of $[Cu(NH_3)_4]^{2+}$ as $[Cu(CN)_4]^{2-}$ did not form.

Test for p or n nature of the doped TiO_2 was performed by photolysis of $[Fe(CN)_6]^{3-}$. The potential of the working electrode was fixed at 100 mV more positive than the oxidation potential of $[Fe(CN)_6]^{4-}$ to guarantee full oxidation of the ferrocyanide. The current due to the oxidation of $[Fe(CN)_6]^{3-}$ collected by the working electrode during the photolysis process is a measure of the photocurrent. This test proved that the doped TiO_2 suspensions have a dual character (p and n). This is because in $[Fe(CN)_6]^{4-}$ we recorded oxidation current, and in $[Fe(CN)_6]^{3-}$ we recorded reduction current. The following equation is used to calculate H_2 rate:

$$H_2 \text{ rate (mol m}^2\text{ h)} = \frac{i \times 10{,}000 \times 3600}{2 \times 96{,}500 \times a}, \qquad (3)$$

where i is the photocurrent (in A), a the electrode surface area, the numbers 3600 corresponding to 1 h (in s), 10,000 corresponding to 1 m^2 and 96,500 C = 1 Faraday.

Reflectance spectra of solid nanoparticles of TiO_2 containing different ratios of V_2O_5 were obtained. The results displayed in Figure 2 are for TiO_2 doped with 10% V_2O_5;

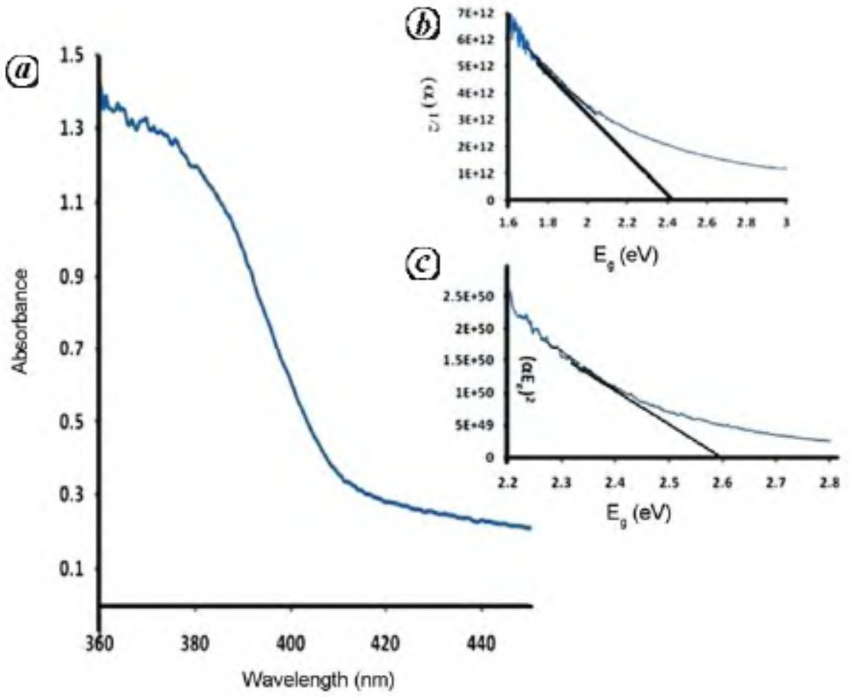

Figure 2. ***a***, Steady-state reflectance spectra for TiO_2 doped with 10% V_2O_5. ***b***, Tauc plots for indirect band gap. ***c***, Tauc plots for direct band gap.

the behaviour of other mixtures was similar, but not identical to that displayed in Figure 2. Direct and indirect band gap transitions were determined following published work[29]. The results indicate an indirect band gap of $E_g \approx 2.4$ eV (intercept of Figure 2 *b*). This is smaller than the direct band gap with a value of $E_g \approx 2.6$ eV (intercept of Figure 2 *c*), which is likely to be the accurate value of the band gap of the doped TiO_2. This suggests that the doped TiO_2 has both direct and indirect band gap transitions when doped with V^{+5}. It is known that the depletion layer width decreases with increasing distance between the energy level of the doping material and the conduction band. The V, Zn and Mg oxides dopant energy levels are not located much farther from the conduction band of TiO_2. This increases the depletion layer width and consequently enhances the charge transfer at the TiO_2/electrolyte interface.

It is well known that for indirect transition three entities are needed to interact in order to proceed: an electron, a photon and a phonon. Interaction with these three entities causes indirect transition to take place at a much slower rate than the direct transition. This also causes the electron–hole recombination process to be much slower than that in an indirect transition band gap. This is because the electron–hole recombination process has to be mediated by the phonons. Such an effect will enhance the photo-conversion efficiencies of the photonic process that takes place at the interface of these doped oxides suspensions.

Doping of TiO_2 with V_2O_5, results in the formation of a bi-function titanium oxide semiconductor. In the presence of hole-scavengers, such as tartarates or borates, charge separation becomes more efficient. Furthermore, as mentioned above, the dopants cause indirect band transitions. The magnitude of these indirect transitions can have a direct effect on the photonic responses of these doped titanium (IV) oxides.

Photolysis of aqueous $[Fe(CN)_6]^{4-}$ results in the formation of hydrated electrons e_{aq^-} and oxidation to $[Fe(CN)_6]^{3-}$. Due to the irreversible nature of this reaction (eq. (1)), when all the $[Fe(CN)_6]^{4-}$ is oxidized to $[Fe(CN)_6]^{3-}$, the hydrated electrons are no longer generated. Reversal of the process represented by eq. (1) is possible by illumination of doped titanium (IV) oxide particles (•) in the presence of a hole-scavenger (X^{2-}) such as borate ($B_4O_7^{2-}$), tartarate ($K[C_2H_2(OH)_2(COO)_2]^{2-}$) or phosphate ($HPO_4^{2-}$). Reduction of $[Fe(CN)_6]^{3-}$ is possible as represented by this reaction:

$$\bullet + h\nu + X^{2-} + [Fe(CN)_6]^{3-} = X^{1-} + [Fe(CN)_6]^{4-}. \quad (4)$$

The rate of reaction of eq. (1) is greater than that of eq. (4) due to the heterogeneity factor and the nature of the indirect band transitions of the semiconductor oxide particles. Co-existence of doped titanium (IV) oxide particles with ferro-cyanide anions under illumination allows continuity in the production of hydrogen. This can be identified by preventing the photocurrent to drop back to lower value after reaching a maximum. This will be the criterion for the comparison of one oxide with another.

Figure 3 is a plot of photocurrent versus time for the photolysis of aqueous electrolytes containing $[Fe(CN)_6]^{4-}$

in phosphate buffer (pH = 10) (trace a), in the presence of pure TiO_2 nanoparticles (trace b) and in the presence of pure TiO_2 doped with 10% V_2O_5 (trace c). The effect of either pure or doped TiO_2 can be noticed in (i) increased photocurrent after the peak time (ca. 350 s) and (ii) greater peak currents generated (traces b and c, Figure 2) than those observed in homogenous electrolytes containing $[Fe(CN)_6]^{4-}$ only (trace a). Photolysis in other studied buffers (tartarates, borates) generates similar results, but not identical to those displayed in Figure 3. From now on, we will only display the plots for calculated H_2 production rate versus time for the studied systems.

Whereas eq. (3) explains the increase in the photocurrent after the peak time, the second observation can be interpreted considering the following.

Upon addition of TiO_2 nanoparticles, both $[Fe(CN)_6]^{4-}$ and $[Fe(CN)_6]^{3-}$ (generated through eq. (2)) were competitively adsorbed on the nanoparticle surface. The modified surface of the nanoparticles enhances the kinetics of reaction represented by eq. (1) by providing an environment for better orientation for the reacting species.

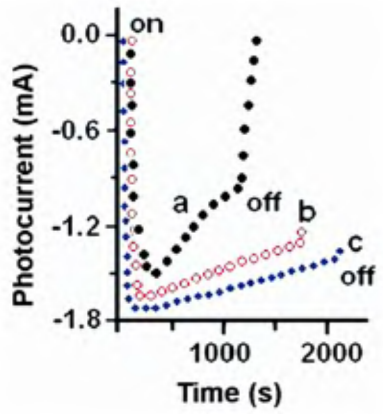

Figure 3. Plot of photocurrent versus time for the photolysis of aqueous electrolytes (a) containing 10 mM $[Fe(CN)_6]^{4-}$ in phosphate buffer (pH = 10), (b) in the presence of pure TiO_2 nanoparticles and (c) in the presence of pure TiO_2 doped with 10% V_2O_5.

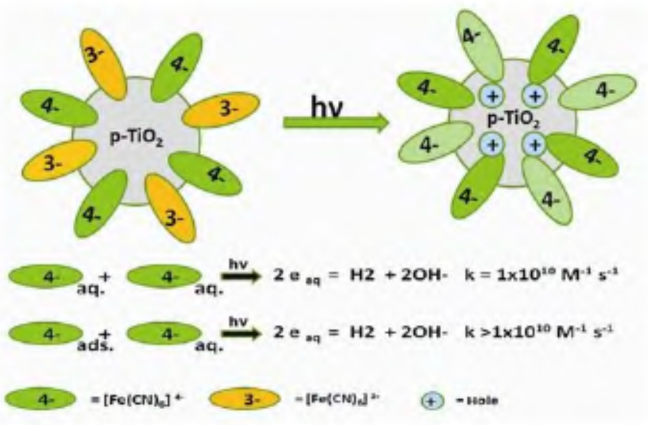

Figure 4. Schematic representation of the adsorption process.

Figure 4 shows the suggested mechanism by which the TiO_2 nanoparticle interfaces catalyse the generation of solvated electrons. As orientation plays an important role in the reaction kinetics, the adsorption of $[Fe(CN)_6]^{4-}$ on TiO_2 particles certainly offers a more effective collision with free $[Fe(CN)_6]^{4-}$. This will enhance the rate by which the reaction represented by eq. (1) proceeds.

Figures 5 and 6 show that in the presence of TiO_2 the calculated hydrogen production rates are greater than those calculated in homogenous electrolytes containing $[Fe(CN)_6]^{4-}$ only. The objective of doping TiO_2 with V_2O_5 is to create metal-oxide assemblies capable of electron–hole production when illuminated with visible light. Figure 5 shows that adding colloidal nanoparticles results in a better rate in hydrogen production (trace b) than that in a basic phosphate buffer containing $K_4[Fe(CN)_6]$ (trace a). However, when TiO_2 doped with 5% V_2O_5 is used, the highest hydrogen production rate is observed (trace c). TiO_2 doped with 10% and 15% V_2O_5 generated lower rates than 5% samples, but still more than that reported with the homogenous $K_4[Fe(CN)_6]$. Such behaviour was expected because with TiO_2 only, the high band gap (3.3 eV) allows only small wavelength UV light ($\lambda < 400$ nm) to be absorbed. Because of the low UV intensity generated by the used solar simulator, small photonic activities of the suspended nanoparticles will take place. However, the photocurrent of TiO_2 doped with 5% V_2O_5 was the highest among other studied samples. This indicates that in phosphate buffer, 5% V_2O_5 supplied the highest surface state density introduced by the diffusion of vanadium ions[33] and decreased the rate of electron–hole recombination due to change in the band transition mechanism from direct to indirect.

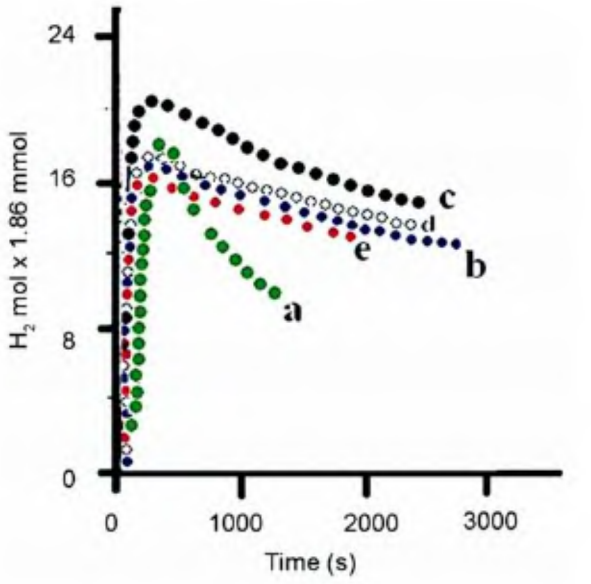

Figure 5. Rate of hydrogen production versus time in only 10 mM of $K_4[Fe(CN)_6]$ in 0.2 M basic phosphate buffer. (a) Oxide-free media; (b) For TiO_2 only; (c) For TiO_2 only doped with 5% V_2O_5; (d) For TiO_2 doped with 10% V_2O_5 and (e) For TiO_2 doped with 15% V_2O_5.

Because the sample of TiO_2 doped with 10% V_2O_5 shows longer time required for steady state photocurrent, we listed the amount of recorded photocurrent for each of studied buffers containing this sample. When borate was used as a buffering medium for the photolysis of TiO_2 doped with different percentages of V_2O_5, the photocurrent recorded for 10% V_2O_5 dopant was the greatest. Such results are different from those observed in phosphate buffer as shown in Figure 5. However, the calculated H_2 production rate in borates (Figure 6) and tartarates (results similar to those of borates) was less than that recorded in phosphates (note the *Y*-axis scales in Figures 5 and 6). The effect of borate, phosphate and tartarate anions on the selective production of hydrogen by TiO_2 doped with 10% V_2O_5 was further studied. The recorded photocurrent during the illumination of 10 mM of $K_4[Fe(CN)_6]$ in 0.2 M solution of these anions at pH 10 was used as an indicator for this effect. The results recorded in Table 1 show that phosphate give the greatest photocurrent. Borate and tartarate give equal effects. Further studies are needed to explain such behaviour and correlate the photonic behaviour with certain properties of the polyanion species, such as molecular orbital structures.

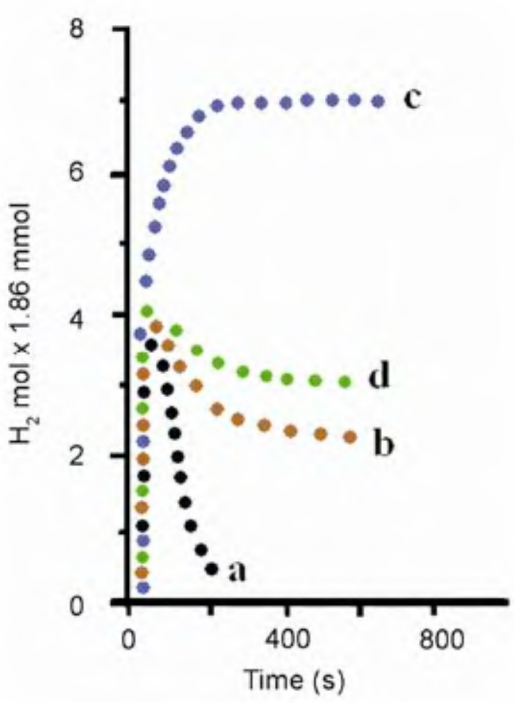

Figure 6. Rate of hydrogen production versus time in only 10 mM of $K_4[Fe(CN)_6]$ in 0.2 M basic borate buffer. (a) Oxide-free media; (b) For TiO_2; (c) For TiO_2 doped with 5% V_2O_5 and (d) For TiO_2 doped with 15% V_2O_5.

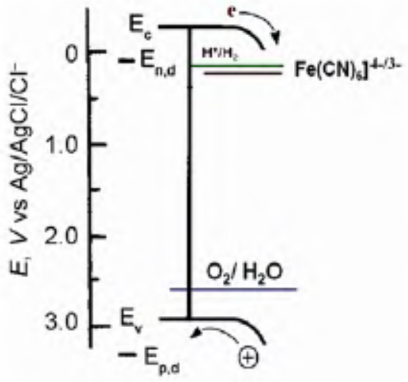

Figure 7. Energy diagram of p-TiO_2 nanoparticles in basic buffered $K_4[Fe(CN)_6]$.

Table 1. Steady state photocurrent for studied metal oxide nanoparticles at pH = 10 in different polyatomic anions (hole-scavengers)

Anion	TiO_2 (10% V_2O_5) ($Am^{-2}\ h^{-1}$)
Tartarate ($K[C_2H_2(OH)_2(COO)_2]^{2-}$)	0.698
Borate ($(B_4O_7)^{2-}$)	0.699
Phosphate ($(HPO_4)^{2-}$)	1.596

The oriented nature of the d-orbital of Fe central atom and the geometry of $[Fe(CN)_6]^{4-}$ makes the outer sphere charge transfer much easier in $[Fe(CN)_6]^{4-}$. This suggests that $[Fe(CN)_6]^{4-}$ can act as a hole-scavenger and compete with buffers oxoanions (X^{2-}). For the measured photocurrent, each 2 photons are consumed; one H_2 molecule is produced according to the following overall photolysis equation.

$$\bullet + h\nu + 2e + 2H_9O_4^+ + 2(h^+) + 2[Fe(CN)_6]^{4-} = 2[Fe(CN)_6]^{3-} + H_2 + 8H_2O. \quad (5)$$

The major effect of V_2O_5 can be qualitatively identified by two important observations: (i) more efficient photoresponse (more hydrogen production) was reported when nanoparticles of TiO_2 doped with V_2O_5 were suspended in buffered basic $[Fe(CN)_6]^{4-}$; (ii) reproducible reactivity of these aqueous suspensions for a long time without deactivation which reflects stability against photo-corrosion. Our studies indicate that TiO_2 doped with 5% V_2O_5 provides the greatest effect in phosphate buffer. Furthermore, phosphate buffer offers the best medium for hole-scavengers among the used anions. Vanadium (V^{+5}) facilitates the transfer of charge carriers at the interface because of alteration of the flat-band potential, and increases the absorption of incident light energy as a result of the increase in depletion layer width at the junction[34]. V^{+5} also provides high density of states that lowers the band gap of TiO_2 and changes its band gap transition from direct to indirect. The stability of the nanoparticles can be explained considering the stability rules in aqueous solutions. These rules state that the E_{pd} (free energy of oxidation the oxide) must be greater than the oxidation of water (E_{OH^-/H_2O}) and the E_{nd} (free energy of reduction of the oxide) is smaller than the reduction potential of H^+ (E_{H^+/H_2O}). The energy diagram in Figure 7 shows that larger band gap of the studied p-type TiO_2 offers an energy map in which a VB and CB energy shifts to the energy

edge where E_{OH^-/H_2O} is less than the E_{pd} (free energy of oxidation of iron oxide) and where E_{H^+/H_2O} is greater than the E_{nd} (free energy of reduction of titanium oxide).

Our study shows that photolysis of water can be more efficient in the presence of a hydrated electron supplier that can be regenerated by photolysis of TiO_2 doped with V_2O_5. In general, percentages of V_2O_5 dopant in TiO_2 greater than 5 do not create a tangible improvement in the photo-activities of TiO_2. The aqueous nanosystems we have used retained their stability as indicated by the reproducibility of their photocatalytic activities.

1. Zhang, Y. J., Yan, W., Pei, W. Y. and Wang, Z. H., Synthesis of TiO_2 nanotubes coupled with CdS. *Mater. Lett.*, 2008, **62**(23), 3846–3848.
2. Ryu, S. Y., Choi, J., Balcerski, W., Lee, T. K. and Hoffmann, M. R., Photocatalytic production of H_2 on nanocomposite catalysts. *Ind. Eng. Chem. Res.*, 2007, **46**(23), 7476–7488.
3. Lindgren, T., Vayssieres, L., Wang, H. and Lindquist, S. E., The emergence of a new generation of smart materials. *Chem. Phys. Nanostruct. Semicond.*, 2003, **4**, 83–110.
4. Jang, J. S., Kim, H. G., Reddy, V. R., Bae, S. W., Ji, S. M. and Lee, J. S., Highly donor-doped (110) layered perovskite as novel photocatalysts. *J. Catal.*, 2005, **231**(1), 213–222.
5. Sartoretti, C. J., Alexander, B., Slarska, D. R., Rutkowska, I. A., Augustynski, J. and Cerny, R., Photoelectrochemical oxidation of water at transparent ferric oxide film electrodes. *J. Phys. Chem. B*, 2005, **109**, 13685–13692.
6. Tabata, S., Nishida, H., Masaki, Y. and Tabata, K., Synthesis of titania-supported platinum catalyst. *Catal. Lett.*, 1995, **34**, 245–249.
7. Maeda, K., Teramura, K., Lu, D., Saito, N., Inoue, Y. and Domen, K., Noble-metal/Cr_2O_3 core/shell nanoparticle as a co-catalyst for photocatalytic overall water splitting. *Angew. Chem., Int. Ed. Engl.*, 2006, **45**(46), 7806–7809.
8. Bard, A. J. and Fox, M. A., Artificial photosynthesis: solar splitting of water to hydrogen and oxygen. *Acc. Chem. Res.*, 1995, **28**, 141–145.
9. Takata, T., Furumi, Y., Shinohara, K., Tanaka, A., Hara, M., Kondo, J. N. and Domen, K., Preparation of $K_2La_2Ti_3O_{10}$ by polymerized complex. *Chem. Mater.*, 1997, **9**, 1063–1069.
10. Sartoretti, C. J., Ulmann, M., Alexander, B. D. and Augustynski, B. D., Nanostructured α-Fe_2O_3 electrodes for solar driven water splitting. *J. Chem. Phys. Lett.*, 2003, **376**, 194–200.
11. Mills, A. and Porter, G., Photosensitized dissociation of water using dispersed. *J. Chem. Soc., Faraday Trans. 1*, 1982, **78**, 3659–3665.
12. Graetzel, M., Bifacial dye-sensitized solar cells based on an ionic liquid. *Nature*, 2001, **414**, 338.
13. Graetzel, M., Nanocrystalline electronic junctions. In *Semiconductor Nanoclusters – Physical, Chemical and Catalytic Aspects* (eds Kamat, P. V. and Meisel, D.), Elsevier, Amsterdam, 1997, p. 353.
14. Goidas, K. R., Bohorques, M. and Kamat, P., Photophysical and photochemical aspects of coupled semiconductors. *J. Phys. Chem. B*, 1990, **94**, 6435–6440.
15. Vogel, R., Pohl, K. and Weller, H., Photoeletrocatalytic activity of a Cu_2O-loaded self-organized highly oriented TiO_2 nanotubes array electrodes for 4-cholorophenol degradation. *Chem. Phys. Lett.*, 1990, **174**, 241–246.
16. Kohtani, S., Kudo, A. and Sakata, T., Electron transfer processes in nanostructured semiconductor thin films. *Chem. Phys. Lett.*, 1993, **206**, 166–170.
17. Vogel, R., Hoyer, P. and Weller, H., Quantum-sized PbS, CdS, Ag_2S, Sb_2S_3, and Bi_2S_3 particles as sensitizers for various nanoporous wide-bandgap semiconductors. *J. Phys. Chem.*, 1994, **98**, 3183–3188.
18. Plass, R., Pelet, S., Krueger, J., Gratzel, M. and Bach, U., Quantum dots sensitization of organic/inorganic hybrid solar cells. *J. Phys. Chem. B*, 2002, **106**, 7578–7580.
19. Peter, L. M., Wijayantha, K. G. U., Riley, D. J. and Waggett, J. P., Band-edge tuning in self-assembled layers of Bi_2S_3 nanoparticles used to photosynthesize nanocrystalline TiO_2. *J. Phys. Chem. B*, 2003, **107**, 8378–8381.
20. Liu, D. and Kamat, P. V., Photoelectrochemical behavior of thin cadmium selenide and coupled titanic/cadmium selenide semiconductor films. *J. Phys. Chem.*, 1993, **97**, 10769–10773.
21. Matsuo, S., Sakaguchi, N., Yamada, K., Matsuo, T. and Wakita, H., Role in photocatalysis and coordination structure of metal ions adsorbed on titanium dioxide. *Appl. Surf. Sci.*, 2004, **228**, 233–244.
22. Peng, T., Zhao, D., Song, H. and Yan, C., Preparation of lanthana-doped titania nanoparticles with anatase mesoporous walls and high photocatalytic activity. *J. Mol. Catal. A: Chem.*, 2005, **238**, 119–122.
23. Liao, D. L. and Liao, B. Q., Shape, size and photocatalytic activity control of TiO_2 nanoparticles with surfactants. *J. Photochem. Photobiol., A: Chem.*, 2007, **187**(2–3), 363–369.
24. Trapalis, C. C., Keivanidis, P., Kordas, G., Zaharescu, M., Crisan, M., Szatvanyi, A. and Gartner, M., $TiO_2(Fe^{3+})$ nanostructured thin films with antibacterial properties. *Thin Solid Films*, 2003, **433**, 186–190.
25. Saif, M. and Abdel-Mottaleb, M. S. A., Titanium dioxide nanomaterial doped with trivalent lanthanide ions of Tb, Eu and Sm: preparation, characterization and potential applications. *Inorg. Chim. Acta*, 2007, **9/10**, 2863–2874.
26. Mayer, T., Hunger, R., Klein, A. and Jaegermann, W., Engineering the line of electronic energy. *Phys. Status Solidi B*, 2008, **245**(9), 1838–1848.
27. Haque, S. A., Taiho, P., Holmes, A. B. and Durrant, J. R., Transient optical studies of interfacial energetic disorder at nanostructured dye-sensitised inorganic/organic semiconductor heterojunctions. *Chem. Phys. Chem.*, 2003, **4**(1), 89–93.
28. Gordon, S., Hars, E. J., Matheson, M. S., Rahani, J. and Thomas, J. K., Reaction constants of the hydrated electron. *J. Am. Chem. Soc.*, 1965, **85**, 1375–1377.
29. Ookubo, A., Kanezaki, E. and Ooi, K., ESR, XRD and DRS studies of paramagnetic titanium(3+) ions. *Langmuir*, 1990, **6**(1), 206–209.
30. Yin, R., Zhao, Y., Lu, S., Wang, H., Cao, W. and Fan, Q., Electrocatalytic oxidation of coal on Ti-supported metal oxides. *Electrochim. Acta*, 2009, **55**(1), 46–51.
31. Ikeda, S. *et al.*, Preparation of $K_2La_2Ti_3O_{10}$ by polymerized complex method and photocatalytic decomposition of water. *Chem. Commun.*, 1998, **20**, 2185–2186.
32. Tauc, J. and Menth, A., States in the gap. *J. Non-Cryst. Solids*, 1972, **8–10**, 569–585.
33. Zhao, G., Kozuka, H., Lin, H. and Yoko, T., Preparation and photoelectrochemical properties of $Ti_{1-x}V_xO_2$ solid solution thin film photoelectrodes with gradient bandgap. *Thin Solid Films*, 1999, **340**, 125–131.
34. Saroj Kumari, Tripathi, C., Singh, A. P., Chauhan, D., Shrivastav, R., Dass, S. and Satsangi, V. R., Characterization of Zn-doped hematite thin films for photoelectrochemical splitting of water. *Curr. Sci.*, 2006, **91**(8), 1062–1064.

ACKNOWLEDGEMENT. This work was supported by Indiana University Summer Faculty Fellowship program.

Received 8 May 2009; revised accepted 25 August 2010